HHS Public Access

Author manuscript

Cell Microbiol. Author manuscript; available in PMC 2019 October 01.

Published in final edited form as:

Cell Microbiol. 2018 October ; 20(10): e12868. doi:10.1111/cmi.12868.

Rounding precedes rupture and breakdown of vacuolar membranes minutes before malaria parasite egress from erythrocytes

Svetlana Glushakova[1], **Josh R. Beck**[2,3], **Matthias Garten**[1], **Brad L. Busse**[1], **Armiyaw S. Nasamu**[2], **Tatyana Tenkova-Heuser**[1], **John Heuser**[1], **Daniel E. Goldberg**[2], and **Joshua Zimmerberg**[1,*]

[1]Section on Integrative Biophysics, *Eunice Kennedy Shriver* National Institute of Child Health and Human Development, National Institutes of Health, Bethesda, MD, 20892, USA

[2]Division of Infectious Diseases, Department of Medicine, Washington University, St. Louis, MO, 63110, USA

[3]Department of Biomedical Sciences, Iowa State University, Ames, IA 50010

Abstract

Because Plasmodium falciparum replicates inside of a parasitophorous vacuole (PV) within a human erythrocyte, parasite egress requires the rupture of two limiting-membranes. Parasite Ca2+, kinases, and proteases contribute to efficient egress; their coordination in space and time is not known. Here the kinetics of parasite egress were linked to specific steps with specific compartment markers, using live cell microscopy of parasites expressing PV-targeted fluorescent proteins, and specific egress inhibitors. Several minutes before egress, under control of parasite $[Ca^{2+}]_i$ the parasitophorous vacuole began rounding. Then after ~1.5 minutes, under control of PfPKG and SUB1, there was abrupt rupture of the PV membrane and release of vacuolar contents. Over the next ~6 minutes there was progressive vacuolar membrane deterioration simultaneous with erythrocyte membrane distortion, lasting until the final minute of the egress program when newly-formed parasites mobilized, erythrocyte membranes permeabilized and then ruptured – a dramatic finale to the parasite cycle of replication.

INTRODUCTION

When malaria parasites invade, grow, and multiply inside their host erythrocytes, they separate themselves from the erythrocyte cytoplasm by residing inside a parasitophorous vacuole for nearly the entire duration of the intraerythrocytic developmental cycle (Cowman et al., 2016; De Niz et al., 2017). At the time of egress, two membranes - the parasitophorous vacuolar membrane (PVM) and the erythrocyte plasma membrane (EPM) - have to be breached by the parasites to egress for the initiation of a new replicative cycle. There is a growing understanding that parasite egress and invasion are two multistep events in parasite life orchestrated by multiple players, both regulatory and catalytic, under the

*Correspondence at joshz@helix.nih.gov.

control of parasite signaling systems (Alam et al., 2015; Beeson et al., 2016; Blackman and Carruthers, 2013; Koch and Baum, 2016; Thomas et al., 2018). Egress of merozoites, an invasive asexual form of malaria parasites, from erythrocytes was originally described by W. Trager as an explosive release of separated parasites from an opening in the erythrocyte membrane (Trager, 1956). Later, recordings of *P. falciparum* egress were made, taking account of the exceptional sensitivity of late-infected erythrocytes to photodamage by light, that documented egress as release of separated parasites from infected erythrocytes (Glushakova et al., 2005). Plasmodium egress is a story of membrane remodeling. The erythrocyte membrane is transformed prior to parasite egress, losing its tension and eventually collapsing onto the schizont (Glushakova et al., 2009, 2005; Hale et al., 2017). It is then thought to be permeabilized by parasite perforins just prior to parasite egress (Glushakova et al., 2010), though the identity of the involved perforins has been elusive (reviewed in (Guerra and Carruthers, 2017)). The erythrocyte membrane curls outward at the site of primary cell opening, a movement that likely helps to eject parasites (Abkarian et al., 2011). The egress time is accompanied by a motion that pushes big membrane fragments of erythrocyte aside while small membranous vesicles are scattered together with released parasites (Glushakova et al., 2005). The potential contribution of mechanical forces leading to rupture of the erythrocyte membrane during parasite egress is unknown. It is possible that an initial limited motility of merozoites (Frénal et al., 2017) could contribute to membrane stretching and fragment the perforated host cell but experimental evidence for this mechanism is missing. However, given how fast the merozoites scatter upon their release from erythrocytes, it has been assumed that the PVM must rupture before, or simultaneously with the erythrocyte membrane and that merozoites must separate from each other prior to egress (Collins et al., 2017; Crick et al., 2013; Glushakova et al., 2005).

Uncertainty about the actual timing of PVM rupture continues to complicate the analysis of the molecular biology of the parasite egress program. Proteins secreted by parasites at the end of the cycle act on their own surfaces, on proteins soluble in the vacuole, or possibly on other targets such as erythrocyte cytoskeleton, within the infected cell. Proteins now known to be involved in egress include kinases (PfPKG - (Collins et al., 2013), PfCDPK5 - (Dvorin et al., 2010)), proteases (PMX - (Nasamu et al., 2017; Pino et al., 2017); SUB1 - (Yeoh et al., 2007), SERA6 - (Ruecker et al., 2012; Thomas et al., 2018, 2016)), pseudo-protease SERA5 (Collins et al., 2017), and the merozoite surface protein MSP1 (Das et al., 2015). The interaction of all these proteins is not fully understood, nor is the time and place of their activity. Recent studies connect PfPKG, PMX and SUB1 activation in a single pathway: PMX and SUB1 are packaged together in secretory organelles of the newly formed merozoites known as exonemes and PMX activates SUB1 hours prior to the end of the cycle (Nasamu et al., 2017). The signal from Ca^{2+} and the elevation of PfPKG leads to secretion of SUB1 from parasite exonemes into the vacuolar space, where it is known to process the PV proteins SERA5 and SERA6 as well as the merozoite surface protein MSP1 (Collins et al., 2013; Das et al., 2015; Ruecker et al., 2012; Yeoh et al., 2007). Inhibition of SUB1 activity (Yeoh et al., 2007), processing (Nasamu et al., 2017; Pino et al., 2017) or SUB1 conditional knockout (Thomas et al., 2018) blocks parasite egress. Inhibition of PfPKG by Compound 2 (C2) blocks SUB1 discharge from the exonemes and also blocks parasite egress, without interference with merozoite maturation or production of mature SUB1, since

the parasite proceeds rapidly to egress upon drug removal (Collins et al., 2013; Taylor et al., 2010). Electron microscopy of schizonts stalled by drugs Compound 1 (C1) or C2 were conflicting, with an early study reporting morphologically breached PVM in C1-inhibited schizonts (Taylor et al., 2010) while another study reported morphologically intact PVM that were functionally perforated after inhibition with drugs C1 or C2 (Hale et al., 2017; Thomas et al., 2018).

Here we analyze and define the kinetics of natural merozoite egress stages using live cell microscopy with and without drug intervention by: 1) visualizing the PVM while minimizing photodamage, 2) testing PVM integrity using a soluble fluorescent probe targeted to the accessible PV space, and 3) measuring the timing of PVM rupture with respect to parasite egress by visualization of PVM membrane and vacuolar soluble content. Monitoring natural egress with these tools revealed a novel stage of the egress program consisting of a dramatic rounding of the PV in preparation for rupture. With drug intervention, we also explore the timing of action and define the effects of egress inhibitors on the status of parasite-enclosing membranes. These results allow us to put ‘time-stamps’ on the vacuolar and erythrocyte membrane transformations, to establish links between the enzymatic processes regulating or performing the individual activities in egress and the morphological steps they control, and to suggest a more precise sequence of events in the parasite egress program.

RESULTS

Independent fluorescent labels and dynamic monitoring of vacuole membrane area, morphology and vacuole content

To observe changes over time to the narrow space between the parasite and vacuole membranes (reviewed in (Bannister et al., 2000)) and to follow the PVM during its transformation, one needs both a fluorescent marker for the vacuolar lumen and a fluorescently tagged PVM-associated protein. The soluble fluorescent protein mRuby3 (Bajar et al., 2016) was expressed under control of the calmodulin promoter and targeted to the vacuolar lumen by gene fusion with the signal peptide of HSP101 (predicted molecular weight of 26.6 kD after signal peptide cleavage). This red luminal marker not only reports the patency of the vacuolar space, it also reports PVM integrity during the final stages of the replicative cycle, by monitoring leakage out of the vacuole. Additionally, we created a separate and distinguishable fluorescent marker to label the PVM itself by engineering a C-terminal mNeonGreen (Shaner et al., 2013) gene fusion to the endogenous Exp2 protein, an integral PVM protein (de Koning-Ward et al., 2009; Glushakova et al., 2017; Johnson et al., 1994). These two markers were distinguishable due to the wide separation in their fluorescence emission spectra.

Co-expression of these constructs allowed observation by dual color confocal live cell microscopy of both the PVM and the PV lumen around the parasites starting from the trophozoite stage of parasite development, in which PVM appeared to surround the developing parasite (Fig.1A). The close juxtaposition of PVM and PPM was preserved during schizogony as expected from electron microscopy images of infected cells (Fig. 1B). During the later stages of schizogony, live-cell time-lapse recordings of the two-color

fluorescence clearly displayed radial ‘ribs’ of mRuby3 that extended down into the gaps between dividing merozoites, as would be expected in the narrow clefts forming between them during invagination of the PPM at the time of cell division (Fig. 1C). The unexpected finding was that the supposed PVM marker Exp2-mNeonGreen was frequently observed in-between dividing merozoites, partially overlapping the distribution of the soluble vacuolar marker mRuby3 (Fig. 1D). We consider the possibility that the PVM itself dips down into the clefts between dividing cells during schizogony, a phenomenon that had not been described in earlier EM analyses of this process (Hanssen et al., 2010; Sakaguchi et al., 2016). A close re-examination of our own electron microscopic images of quick-frozen schizonts freeze-substituted for plastic embedding and thin sectioning, which we considered as true-to-life as possible, failed to detect insertion of PVM clefts in-between dividing merozoites. The PVM apparently sustains its normal peripheral location (Fig. 1B) in all inspected schizonts.

To explain the discrepancy between light and electron microscopic observations of the vacuole membrane we considered a possibility that in addition to its integral membrane form, Exp2-mNeonGreen might exist in a partially soluble form, or even that a portion of the mNeonGreen fusion-construct might be liberated from Exp2 (possibly via proteolytic cleavage in the vacuole) to yield a soluble mNeonGreen signal that would overlap with soluble mRuby3. However, two experimental findings argued against the likelihood of there being some soluble Exp2. First, mRuby3 and Exp2-mNeonGreen labels did not always co-localize, as would be expected for two soluble markers in a continuous PV lumen (Fig. 1D). Second, when the PVM was mildly stretched during live-cell observation (by inducing swelling of the infected erythrocyte and the vacuole, via photodamage to the erythrocyte membrane with a pulse of high-energy light somewhere outside the parasite) the Exp2-mNeonGreen signal in infected cells promptly assumed an exclusively peripheral location, just as the vacuole diameter increased slightly (Fig. 1E, Movie 1). These two sets of data, and the fact that Exp2 is an integral membrane protein argue against there being significant fraction of soluble Exp2-mNeonGreen or free mNeonGreen and support our use of Exp2 as a membrane marker. Future work is needed to identify the electron microscopic correlate of its signal down in-between developing merozoites during schizogony.

Rounding of the PV marks the onset of the mechanical steps in parasite egress program

Since the double-labeled parasites do not have a noticeable growth defect or altered cycle length, they are sufficiently viable for analysis of parasite egress kinetics. Living dual-labeled schizonts, without pharmacological synchronization or cycle interruption, were recorded using time-lapse confocal fluorescence microscopy with low-light intensity to excite mNeonGreen and mRuby3 (0.2 μW light for 488 nm laser and 0.6 μW light for 561 nm laser). Parasite-infected erythrocytes were screened for status of schizogony using DIC confocal microscopy and recordings of the late-infected erythrocytes were initiated up to one hour prior to parasite egress. Sufficient recordings were made to precisely determine the distribution of the duration of each stage of the egress program. When a recording ended in dispersion of released merozoites (Glushakova et al., 2005) the times between the end of each stage and the actual release of the first merozoite was tabulated.

A new stage was seen and validated in all recordings: the parasitophorous vacuole rounded just prior to PVM rupture (Fig.2A). This stage started on average less than 10 min before egress, lasted 1-2 minutes (1.60+/−0.21 min, mean +/− SEM, n=27, Fig. 2B) and appeared in two-dimensional fluorescence images as a transformation of the PVM-enclosed parasites from an asymmetrical to a circular object. Remarkably, the PVM-Exp2 signal was observed to gradually move to the vacuole periphery during this stage (Movie 2), despite the ongoing enclosure of each future merozoite with PPM. To check for the loss or gain of Exp2 during rounding, the Exp2-mNeonGreen signal of random optical sections was integrated before and during the rounding stage, but no changes were observed (Supplementary Fig.1). Nor did the pattern of the soluble PV marker change during PVM rounding (Fig. 2C). During this stage, the PVM preserves its integrity, as we can see by the continuing containment of soluble mRuby3 protein inside the vacuole. Likewise, PV-mRuby3 signal levels were stable up to 1 hour prior to vacuole rounding, indicating that the PVM integrity was not compromised prior to and during the rounding stage (17 experiments, 36 recordings of parasite egress; Fig. 2D–E). Taken together, these observations suggest that a drastic remodeling of the PVM starts about the time that merozoite morphogenesis is finished but does not affect the PVM barrier. Merozoites were still tightly associated with each other inside the rounded vacuole and observed as one flower-like arrangement. Since the vacuole rounding stage is seen in every single recording, it appears to be an obligatory stage in parasite egress.

The observed PV rounding could result from some sort of osmotic swelling of the vacuole, since our experiments to induce PV rounding also led to consolidation of Exp2-mNeonGreen to the periphery. To determine if the vacuole indeed swells during the natural rounding stage prior to rupture, we acquired Z-stacks of schizont fluorescent images prior to and during the rounded stage and carried out volumetric analyses of vacuoles in 5 recordings of parasite egress by two independent methods. Irrespective of the analytical method we chose, we could not in fact detect any increase in vacuolar volume. Rather, we calculated a slight *decrease* in vacuolar volume during the transient rounding stage, barely significant (p=0.038) in our mask-based analysis but not significant in our threshold analysis method (Fig. 2F). Still, both analyses clearly confirmed the increase in vacuole sphericity that we observed, i.e. a decreased vacuolar surface area to vacuolar volume ratio in the mask-based method, p=0.01 or smaller ellipsoid fit error (χ^2) in the threshold method, p=0.046 during the rounded stage (Fig.2G). Thus, these analyses did not support the idea that the PV swells during the rounding stage, but rather suggested that the PV membrane must decline in surface-area for the PV to become more spherical with practically the same volume. One way this could happen without the PVM actually losing its integrity would be if small vesicles trafficked away from it during the increase in rounding and sphericity. We did not observe such vesicles, but they might be too small to see by light microscopy and too transient to see by electron microscopy. Notwithstanding, we can conclude that the PV rounding is not due to swelling.

PVM rupture is marked by loss of soluble contents and followed by piecemeal PVM degradation and erythrocyte membrane transformation

Our time-lapse recordings of natural parasite egress provided clear-cut views of PVM rupture and degradation, allowing us to define the timing between vacuole rupture and parasite egress, and to link PVM rupture with progressive collapse of the erythrocyte membrane. We reproducibly observed the stages described below. The brief stage of vacuole rounding was always followed by PVM rupture, accompanied by a sudden drop of mRuby3 fluorescence around the schizont and the spread of mRuby3 signal throughout the entire erythrocyte, indicating the release of soluble PV content from the vacuole (Fig.3A–B, Movie 3). In most recordings, the PVM ruptured between 5-8 min prior to parasite egress (6.54+/−1.85 min, mean +/−SEM, n=27, 11 independent experiments; Fig. 3C). To control for potential deleterious effects of our observing PVM rupture in schizonts expressing fluorescent proteins, e.g, photodamage from our double laser illumination, two additional sets of recordings were made with single-tagged parasites and single laser illumination. Both double and single-laser illumination datasets gave comparable results (Supplementary Fig. 2). Qualitatively, all the features we detected at each stage of egress, as well as the sequence of these stages, were the same, independent of the mNeonGreen and mRuby3 reporters or the nature of the illumination.

The PVM appeared to break first in one or a few places, then immediately relaxed and began to decompose, often progressively from the broken regions (Fig. 3A, Movie 4). PVM degradation lasted several minutes, albeit at different rates in different cells. Eventually, the PVM transformed into membrane fragments of variable sizes, supporting the previously reported electron microscopy images of schizonts in which parasite egress from the erythrocyte was blocked by the cysteine protease inhibitor E64 (Glushakova et al., 2009; Hale et al., 2017). To test the preservation of EXP2-coupled fluorescence during egress time we magnet-purified late schizonts and assessed the size of EXP2 by immunoblot analysis. Isolated schizonts immediately proceed to parasite egress, if returned to the physiological conditions, indicating the presence of schizonts at the very last minutes of cycle in such populations (Glushakova: unpublished data from the multiple observations). Practically all of the EXP2-mNeonGreen protein fusion is intact in schizonts as detected by the monoclonal anti-EXP2 antibodies (Fig. 3D), thus making unlikely a scenario of mNeonGreen selective degradation or fusion protein proteolysis as a reason of fluorescence loss in our observations. In most recordings, the merozoites appeared to adhere as one mass right up to the end of PVM degradation, as judged by the preservation of their flower-like architecture and their absence of movement inside the RBC. To monitor whether the signals or activated enzymes that cause PVM rupture could act upon other membranes within the same erythrocyte, we looked for doubly-infected erythrocytes that had two independent PVs and saw that when one schizont initiated its egress program in the presence of a second one that was still immature, the rupture and degradation of the first PVM did not affect the integrity of the other (Fig. 3E). mRuby3 remained encapsulated in the second PV in all 19 cases we recorded (Fig. 3F, Movie 5). Thus, the agents that cause PVM breakage apparently cannot spread to other PVM’s in the same erythrocyte and act on them from outside.

We also observed while monitoring the final stages of egress that PVM breakage was closely linked temporally with agonal changes in the erythrocyte membrane. This was manifest first by ruffling of the erythrocyte membrane, then by its relaxation and gradual collapse onto the schizont body ((Glushakova et al., 2009, 2005); Fig. 3A, Movie 3). Presumably, these changes reflect a degradation of the erythrocyte cytoskeleton by released PV-content. We have seen signs of it before, when we reported changes of the erythrocyte membrane refractive index in DIC images (Glushakova et al., 2009, 2005). This simultaneous PVM degradation and RBC membrane deterioration continued throughout the time between PVM rupture and parasite egress.

The next stage we observed was merozoite separation or the completion of cytokinesis, which generally happened during the very last minute before final egress (although Fig. 3G and Movie 6 show a relatively rare case where the process took a few minutes, so we could clearly observe and record it). Then, immediately prior to egress, we observed frank erythrocyte membrane perforation, which occurred just seconds prior to parasite egress. This we earlier detected by the influx of extracellular phalloidin into infected erythrocytes (Glushakova et al., 2010). Here, with our single and double-labeled iRBCs, we could document RBC perforation by the efflux of mRuby3, since this marker had previously been released from the PV into the erythrocyte cytoplasm, and now could be seen diffusing into the bulk extracellular fluid and totally disappearing. However, unlike the lack of effect of PVM rupture on a second PVM we observed in doubly infected cells, we now saw a profound effect of frank erythrocyte permeation on the integrity of the second vacuole. Its membrane immediately became permeable or ruptured in 67% of cases we observed (12 of 18 recordings) (Fig. 3F, Movie 5). This indicated that soluble lytic agents of EPM breakdown must be active against the PVM.

Finally, we observed of course that the full erythrocytic cycle of parasite development was completed by egress and dispersal of new merozoites from the ruptured erythrocytes.

Intraparasitic free Ca^{2+}, PfPKG, SUB1, and cysteine protease initiate different mechanical steps of parasite egress

To isolate intermediates of egress, we turned to the known macromolecules of egress to determine if their inhibition might block the progression of the egress pathway at well-defined stages. Four inhibitors are known to block egress through independent macromolecules: 1) BAPTA-AM (Glushakova et al., 2013), a chelator of intracellular Ca^{2+} that blocks Ca^{2+-}dependent parasite signaling systems (at least two calcium-dependent kinases are known to be required for egress, PfPKG and PfCDPK5); 2) Compound 2 (C2), which targets PfPKG, a protein kinase implicated in controlling organellar secretion into the PV before egress (Collins et al., 2013); 3) CWHM-117, an inhibitor of PMX, one of the early proteases in the proteolytic cascade leading to parasite egress (Nasamu et al., 2017); 4) and E64, a cysteine protease inhibitor that blocks late events in egress through an unknown target (Glushakova et al., 2009; Salmon et al., 2001).

Chelation of the intracellular Ca^{2+} with BAPTA-AM within the last two hours of replicative cycle gave the earliest intervention effect: the developmental cycle was blocked prior to the vacuole rounding stage (Fig. 4A). BAPTA-AM inhibited 90% of egress events at 60 μM

(Fig. 4B) and all inspected cells preserved EPM (see WGA-Alexa 647-labeled erythrocyte surface) and 93% of inspected stalled schizonts (n=72) had an intact vacuole and normal parasite morphology.

C2 at 4 μM inhibited the egress program later: drug-treated late schizonts slowly progressed towards the stage of the rounded vacuole but did not proceed beyond it (Fig. 4A). Schizonts affected by drug within the last 10-15 minutes of the cycle were stalled on the rounded vacuole stage but became morphologically distorted upon the prolonged treatment. 96% of inspected cells treated with C2 (n=70) had an intact vacuole that often looked enlarged and sometimes had extruded PVM blebs. Despite vacuole stretching, 90% of stalled schizonts with a distorted morphology (n=67) maintained the mRuby3 signal within vacuole, indicating preserved PVM integrity inside these cells. The EPM was preserved in C2-treated cells (Fig. 4A, WGA panels). Kinetic studies showed a quick inhibitory effect of C2 on parasite egress: at 4 μM C2, egress was blocked for 95% of infected cells within a few minutes post application (Fig. 4B–C). We also confirmed by a quantitative egress assay the reversibility of the C2 inhibitory effect, as drug withdrawal led to elevated parasite egress compared to the untreated control cultures (Fig. 4B).

We previously observed that CWHM-117, an inhibitor of SUB1 processing, leads to the full inhibition of parasite egress at a concentration of 0.5 μM in parasites with PMX knockdown (KD) (Nasamu et al., 2017). However, the effect was observed only if the KD was initiated and the drug was administered well before the end of parasite cycle, reflecting the timing of PMX activity. Here we repeated these experiments with NF54-PMX-KD-Exp2-mNeonGreen parasites to visualize the PVM. CWHM-117-treated cultures accumulated stalled schizonts with a distorted morphology. The PVM of these schizonts was intact in 82% of inspected infected cells (n=91) and the vacuole looked rounded and enlarged (Fig. 4D). Thus, fully blocked SUB1 processing leads to the abortive end of parasite development at the stage of the rounded vacuole. C2 and CWHM-117-treated distorted schizonts had a similar distorted morphology and both have preserved intact erythrocyte membrane detected by WGA-Alexa 647 labeling (Fig. 4A, D).

Finally, we visualized the status of the PVM in merozoite clusters accumulated during E64 treatment of late-stage parasites (Glushakova et al., 2009). The PVM was broken in 97% of clusters captured inside erythrocytes (n=110), while the erythrocyte plasma membrane was permeable but integral (Fig. 4A, last two cells). This implicates cysteine protease(s) in the erythrocyte membrane rupture needed for successful parasite egress.

DISCUSSION

A canonical sequence of mechanical events was reproducibly observed during the last 10 minutes of intraerythrocytic cycle of malaria parasite replication leading to parasite egress from the infected cell. The first short step, rounding of parasitophorous vacuole containing mature parasites, was followed by abrupt PVM rupture initiating its subsequent slow degradation in parallel with gradual collapse of erythrocyte membrane. The final set of events at the very last minute of the cycle included merozoite separation, erythrocyte

membrane permeation and rupture. Release of dispersed parasites completed the replicative cycle.

Timing and pattern of vacuolar membrane degradation in the natural parasite egress

The results described above depended upon and illustrated the utility of a dually-labelled, gene-edited *Plasmodium falciparum* expressing genetically encoded markers for the PV and PVM. The labeled vacuole revealed a remarkable PVM reorganization during the initiation of the egress program: a newly appreciated stage of vacuole rounding, lasting 1-2 minutes and leading to increased vacuolar sphericity without swelling. Such phenomenon has precedents in the condensing granule phase of pancreatic and other large granular exocytosis and is caused by retrieval of membrane vesicles from the maturing secretory granule (Bonnemaison et al., 2014), a phenomenon still not observed in our electron micrographs of parasite-infected erythrocytes. This rounding of the parasitophorous vacuole depended upon intracellular Ca^{2+}, which presumably activates Ca^{2+}-dependent enzymes working on this stage, but apparently not PfPKG, since rounding happens albeit with slow kinetics in cultures treated with PfPKG inhibitor Compound 2.

The rounded stage was followed by the abrupt rupture of the vacuolar membrane, starting approximately 5-8 minutes prior to egress. Secretion of the fully processed SUB1 protease from parasite exonemes into the vacuolar lumen is a prerequisite for vacuolar membrane rupture. Two of four tested interventions into the egress program blocked parasite egress at the rounded vacuole stage. Both implicate SUB1 activity in the vacuolar lumen in the process of PVM rupture: i) interference with SUB1 processing (PMX-KD + CWHM-117) or ii) block of SUB1 secretion into the vacuolar lumen (C2) each independently stalled schizonts inside a rounded vacuole. Under the pressure of these interventions, the vacuole often became enlarged and vacuolar membrane sometimes partially extruded from the erythrocyte as a bleb, however PVM still preserved its integrity and was impermeable to protein mRuby3. This finding suggests that without SUB1 activation, the PVM lacks sufficient tension to lead to its rupture. In accord with this notion, our observations suggest that the products of SUB1 activity include membrane-active agents of PVM rupture, enzymatic or lytic. First, PVM degradation has a progressive pattern, takes several minutes, occurs with the broken, i.e. relaxed membrane and produces membrane fragments distributed in the erythrocyte cytoplasm, but does not fully consume the PVM. Second, PVM degradation does not affect merozoites plasma membrane or PVM of the second vacuole, in doubly-infected erythrocytes. This suggests that the membrane disrupting activity is site-specific and/or insufficient in quantity to perturb a second mass of PVM (see also review by (Guerra and Carruthers, 2017)). Production of membrane-active peptides or activation of a secreted phospholipase (reviewed in Flammersfeld et al., 2017) could break down the PVM. Importantly, one parasite phospholipase has been shown in *P. berghei* to localize to the liver-stage PVM, and disruption of this enzyme produced a defect in liver-stage PVM rupture and egress (Burda et al., 2015).

Visualization of PV and PVM in the live cell recordings of natural parasite egress allowed us to re-evaluate the recently published data suggesting PVM permeation 10-30 minutes prior to vacuole rupture and parasite egress (Hale et al., 2017). This time interval was carefully

explored in our work. Not one of the multiple recordings of natural parasite egress shows evidence of mRuby3 leakage from the PV prior to PVM rupture that happens 5-8 minutes prior to parasite egress. This discrepancy could be explained by the relatively slow kinetics of PVM degradation we observed. As a result, some big fragments of the broken PV membrane would be observed as intact membrane in electron microscopy of single ultrathin sections used by Halle et al., while the membrane defect may remain undetected. A potential detrimental effect of the prolonged C2 treatment on PVM integrity in infected cells also should be assessed.

In contrast to the PVM degradation, host cell membrane perforation and rupture was associated with permeabilization of the second vacuole in the double-infected erythrocytes, suggesting that the agent of erythrocyte membrane perforation is soluble and acts on both PVM and EPM. This agent has not yet been identified (Guerra and Carruthers, 2017).

Vacuolar membrane rupture is a prerequisite of subsequent steps of parasite egress program

The high precision of estimated time between PVM rupture and parasite egress shows that leakage of vacuolar content into the erythrocyte compartment is tightly associated with an initiation of morphological changes in the infected erythrocyte, described before (Glushakova et al., 2010, 2009, 2005; Hale et al., 2017; Langreth et al., 1978; Thomas et al., 2018; Wickham et al., 2003) but not previously attributed to the PVM rupture. During this interval of time, lasting on average 5-8 minutes, and only after PVM rupture, one sees the degradation of the vacuolar membrane and simultaneous transformation of erythrocyte membrane, observed as a gradual collapse of EPM onto the schizont body, possibly reflecting erythrocyte cytoskeleton digestion (Bowyer et al., 2011; Millholland et al., 2011). Cysteine proteases were implicated in parasite egress: the broad-spectrum cysteine inhibitor E64 blocks parasite egress by acting on an as yet unknown target (Salmon et al., 2001) and preventing erythrocyte membrane rupture (Glushakova et al., 2009). One candidate for the E64-sensitive enzyme and an agent of erythrocyte cytoskeletal digestion is the parasite cysteine protease SERA6, which must be processed by SUB1 prior to PVM rupture and then is released in active form into the erythrocyte compartment upon PVM rupture (Thomas et al., 2018). This possibility is consistent with our data, which showed a very tight temporal association of PVM rupture with the abrupt initiation of the erythrocyte membrane breakdown. Indeed, SERA6 can enzymatically process the major erythrocyte cytoskeleton protein spectrin in vitro, and conditional knockout of SERA6 prevents parasite egress from erythrocyte, mimicking the effect of E64 (Thomas et al., 2018). Combined observations contradict the notion that human calpain-1 protease *alone* is responsible for erythrocyte membrane rupture (Chandramohanadas et al., 2009; Millholland et al., 2011). The data presented here and in recent publications reinforce the need for work on the biochemical identity of all proteases and mechanisms involved in erythrocyte cytoskeleton disruption (Das et al., 2015; Glushakova et al., 2013; Thomas et al., 2018).

In conclusion, the double fluorescent protein labeling of the parasitophorous vacuole and its delimiting membrane allowed a more complete description and sequencing of the events leading to parasite egress than hitherto possible (see figure 5, summarizing the timing,

blocking, and sequence of the stages of egress mechanism discussed here). Calcium initiates parasite egress. A new morphological intermediate, PV rounding, appears to mark a critical point in the egress sequence. SUB1 activity is linked to the rupture of vacuolar membrane. PV rupture is a major event that controls all the stages that follow within the boundary of erythrocyte, leading to successful parasite release from host cells to spread *Plasmodium* infection. The three stages of egress program, i.e. vacuole rounding, vacuole rupture and degradation, and erythrocyte membrane rupture could be independently blocked by pharmacological intervention, thus indicating the applicability of more complex combination therapy for malaria.

EXPERIMENTAL PROCEDURES

Inhibitors

Compound 2 (4-[7-[(dimethylamino)methyl]-2-(4-fluorphenyl) imidazo[1,2-a] pyridine-3-yl]pyrimidin-2-amine; MRT00072329) was provided by Dr. Simon Osborne, Medical Research Council Technology (MRCT), United Kingdom. CWHM-117 was provided by Dr. Marvin Meyers (St. Louis University). E-64, a cysteine protease inhibitor, was purchased from Sigma (E3132). BAPTA-AM was purchased from Invitrogen (B6769).

P. falciparum culture and human erythrocytes

All parasite lines were maintained in culture at low parasitemia in freshly collected human erythrocytes of healthy donors after obtaining their consent to participate in the NIH IRB-approved Research Donor Program in Bethesda, MD (all samples were anonymized). Culture medium composition: RPMI 1640 supplemented with 25 mM HEPES, 0.1 mM hypoxanthine, 25 μg/ml gentamicin, 0.5% Albumax II (Gibco), and 4.5 mg/ml glucose (Sigma).

Generation of parasite lines

PV targeting of mRuby3 was achieved by fusion of the HSP101 signal peptide (SP) to the N-terminus of mRuby3. Sequence encoding the HSP101 signal peptide was inserted into pLN-GFP1-10 (J. R. Beck, unpublished) after the GFP1-10 start codon using primer P1 with a QuickChange Lightning Multi Site-Directed Mutagenesis kit (Agilent). The mRuby3 coding sequence was amplified from the plasmid pKanCMV-mClover3-mRuby3 (Addgene #74252, (Bajar et al., 2016)) with primers P2/3 and inserted between NheI and AflII to replace GFP1-10 and create an HSP101-SP-mRuby3 fusion under the control of the P. falciparum calmodulin promoter. The resulting plasmid, named pLN-HSP101-SP-mRuby3, was co-transfected with pINT (Adjalley et al., 2010) into the previously described NF54attB::Exp2-mNeonGreen parasite line (Glushakova et al., 2017) to facilitate integration into the cg6 locus through integrase mediated attB x attP recombination. Selection with 2.5 μg/ml Blasticidin S was applied 24 hour post transfection. A clonal line displaying both Exp2-mNeonGreen and PV-mRuby3 fluorescence was derived by limiting dilution after parasites returned from selection. For Exp2-mNeonGreen tagging in the PMXapt background, PMXapt parasites (Nasamu et al., 2017) were transfected with pyPM2GT-Exp2-mNeonGreen (Glushakova et al., 2017). Selection with 2 μM DSM-1 was applied 24

hours post transfection (in addition to 2.5 μg/ml Blasticidin S and 1 μM anhydrotetracycline for maintenance of the PMX aptamer system).

Primers—

P 1	CTAATAGAAATATATCACCTAGGATGACAAGAAGATATTTAAAGTATTATATTTTTGTTACTTTATTGTTTTTTGTTCAAGTTATTAATAAT
P 2	ATAATGTATTGTGTGCTAGCGTGTCTAAGGGCGAAGAGCTGATCAAG
P 3	TTATATAACTCGACCTTAAGTTACTTGTACAGCTCGTCCATGCC

Confocal microscopy of infected erythrocytes

Live-cell recording was performed as described elsewhere (Glushakova et al., 2005) using LSM 800 and LSM 880 laser-scanning microscopes (Zeiss) with a 63X 1.4 NA oil objective. Cells were illuminated with 488 nm (0.2 μW light) and 561 nm (0.6 μW light) laser to excite mNeonGreen and mRuby3 correspondingly. Erythrocyte surface in the static experiments was labeled using Wheat Germ Agglutinin, Alexa Fluor™ 647 Conjugate, WGA, at concentration 10 μg/ml (Thermo Fisher Scientific) and visualized by 640 nm laser illumination. To observe parasite egress, infected culture (0.25-1% hematocrit) was placed into environmental chambers suited for microscopy (HybriWell HBW20, Grace Bio-Labs, Inc.). Time-lapse recording of parasite egress was performed with the variable intervals between image collection to minimize photodamage. Some recordings were made using Airyscan confocal microscopy. In this case the optimal pixel size was selected according to Zen software recommendations (Zeiss) and processed using the ‘auto filter’ setting. The photo-wounding of infected erythrocytes was performed using the 800 nm two-photon laser illumination (Chameleon, Coherent) at 50% power (0.8 μs pixel dwell time, 1μm circle area of illumination with 10 iterations).

Electron microscopy

Malaria-infected erythrocyte cultures were preserved in their most natural, lifelike state by quick-freezing them against a homemade “cryopress” that consisted of a copper block cooled with liquid helium (Heuser et al., 1979). Thereafter, they were freeze-substituted by classical means (Feder and Sidman, 1958) in acetone containing 4% OsO_4, but with an accelerated 12 hours of rotation and progressive warm-up from −95°C to −10°C. Then they were rinsed in room temperature acetone and mordanted with 0.5% tannic acid (Sigma, MW1500) before staining with 0.5% uranyl acetate in acetone for 1h at room temperature. Finally, they were embedded in classical English Araldite epoxy resin via progressive substitution of acetone with epoxy, and then strong vacuum-extraction of any residual acetone with a high vacuum at 70°C. After 12 hours of 70°C polymerization, plastic sections were cut at 80 nm thickness and stained with 0.3% lead citrate in 0.1M NaOH for 5 min, before viewing at 80 KV in a standard electron microscope, and photography with a 6Kx8K pixel AMT bottom-mount EM-camera.

Immunoblot analysis

For Immunoblots to monitor the integrity of the EXP2-mNeonGreen fusion protein, schizonts were magnet-purified using an LD column and quadro MACS system (Miltenyi Biotech). Purified schizonts were then either directly processed for Western blot or first treated with PBS containing 0.025% saponin. Blots were probed with monoclonal mouse anti-EXP2 antibody clone 7.7 (Hall et al., 1983) used at a dilution of 1:1000. Primary antibodies were detected with IRDye 800-conjugated secondary antibodies used at a 1:10,000 dilution and blots were visualized using an Odyssey infrared imaging system (Li-COR Biosciences).

Quantitative parasite egress assay

To quantify the effect of drugs on egress, infected cells were treated with drugs in chambers at 37°C to accumulate egress sites, and then chambers were cooled at 15°C for 30 minutes to stop parasite egress. Egress was quantified as the fraction of schizonts releasing merozoites. Images of stalled schizonts were taken at 37°C to confirm the block of cycle progression.

Quantitative image analysis

Vacuole volume and sphericity estimates were derived independently using two approaches of image analysis of Z stacks fluorescence: a threshold-based and a mask-based approach. Threshold-based approach: The vacuole volume was estimated using a Matlab (Version2015b, MathWorks) script. Briefly, a maximum projection of the Exp2-mNeonGreen z-stack was thresholded using the Otsu method (Otsu, 1979). The threshold from the projection was then applied to each slice. The outline was then filled and smoothed by a dilate-erode-dilate step giving a vacuole cross-section. The vacuole volume was measured by summing up the cross-section areas multiplied by the pixel height. The vacuole volume and sphericity were further estimated by fitting an ellipse (ellipsoid_fit.mat, Yury Petrov, Oculus VR) to the outline of the cross-sections. Mask-based approach: manual masking was used to estimate the vacuole volume. Briefly, each section of the Z stack images was segmented manually using FIJI image analysis software (Schindelin et al., 2012). This generated a volumetric mask, which was analyzed in Python using the SciPy (Jones et al., 2001) and scikit-image (van der Walt et al., 2014) libraries. Mask volume was determined by summing the masked voxels. Surface area was determined by convolving the mask with the kernel [−1,1] in each axis (x,y,z), adding together the areas of the respective facets of the non-zero voxels.

Supplementary Material

Refer to Web version on PubMed Central for supplementary material.

Acknowledgments

We thank Robyn Roth for assistance with sample preparation for electron microscopy, Alan Hoofring for artwork, and Kamran Melikov for fruitful discussion. This study was funded by the Intramural Research Programs of the *Eunice Kennedy Shriver* National Institute of Child Health and Human Development. Daniel E. Goldberg and Josh R. Beck acknowledge funding from the National Institutes of Health including K99/R00 HL133453 to Josh R. Beck and RO1 AI138447 to Daniel E. Goldberg.

References

Abkarian M, Massiera G, Berry L, Roques M, Braun-Breton C. 2011; A novel mechanism for egress of malarial parasites from red blood cells. Blood. 117:4118–4124. DOI: 10.1182/blood-2010-08-299883 [PubMed: 21297002]

Adjalley SH, Lee MCS, Fidock DA. 2010; A method for rapid genetic integration into Plasmodium falciparum utilizing mycobacteriophage Bxb1 integrase. Methods Mol Biol Clifton NJ. 634:87–100. DOI: 10.1007/978-1-60761-652-8_6

Alam MM, Solyakov L, Bottrill AR, Flueck C, Siddiqui FA, Singh S, Mistry S, Viskaduraki M, Lee K, Hopp CS, Chitnis CE, Doerig C, Moon RW, Green JL, Holder AA, Baker DA, Tobin AB. 2015; Phosphoproteomics reveals malaria parasite Protein Kinase G as a signalling hub regulating egress and invasion. Nat Commun. 6:7285.doi: 10.1038/ncomms8285 [PubMed: 26149123]

Bajar BT, Wang ES, Lam AJ, Kim BB, Jacobs CL, Howe ES, Davidson MW, Lin MZ, Chu J. 2016; Improving brightness and photostability of green and red fluorescent proteins for live cell imaging and FRET reporting. Sci Rep. 6:20889.doi: 10.1038/srep20889 [PubMed: 26879144]

Bannister LH, Hopkins JM, Fowler RE, Krishna S, Mitchell GH. 2000; A Brief Illustrated Guide to the Ultrastructure of Plasmodium falciparum Asexual Blood Stages. Parasitol Today. 16:427–433. DOI: 10.1016/S0169-4758(00)01755-5 [PubMed: 11006474]

Beeson JG, Drew DR, Boyle MJ, Feng G, Fowkes FJI, Richards JS. 2016; Merozoite surface proteins in red blood cell invasion, immunity and vaccines against malaria. FEMS Microbiol Rev. 40:343–372. DOI: 10.1093/femsre/fuw001 [PubMed: 26833236]

Blackman MJ, Carruthers VB. 2013; Recent insights into apicomplexan parasite egress provide new views to a kill. Curr Opin Microbiol. 16:459–464. DOI: 10.1016/j.mib.2013.04.008 [PubMed: 23725669]

Bonnemaison M, Bäck N, Lin Y, Bonifacino JS, Mains R, Eipper B. 2014; AP-1A controls secretory granule biogenesis and trafficking of membrane secretory granule proteins. Traffic Cph Den. 15:1099–1121. DOI: 10.1111/tra.12194

Bowyer PW, Simon GM, Cravatt BF, Bogyo M. 2011; Global Profiling of Proteolysis during Rupture of Plasmodium falciparum from the Host Erythrocyte. Mol Cell Proteomics. 10:M110001636.doi: 10.1074/mcp.M110.001636

Burda PC, Roelli MA, Schaffner M, Khan SM, Janse CJ, Heussler VT. 2015; A Plasmodium Phospholipase Is Involved in Disruption of the Liver Stage Parasitophorous Vacuole Membrane. PLOS Pathog. 11:e1004760.doi: 10.1371/journal.ppat.1004760 [PubMed: 25786000]

Chandramohanadas R, Davis PH, Beiting DP, Harbut MB, Darling C, Velmourougane G, Lee MY, Greer PA, Roos DS, Greenbaum DC. 2009; Apicomplexan Parasites Co-Opt Host Calpains to Facilitate Their Escape from Infected Cells. Science. 324:794–797. DOI: 10.1126/science.1171085 [PubMed: 19342550]

Collins CR, Hackett F, Atid J, Tan MSY, Blackman MJ. 2017; The Plasmodium falciparum pseudoprotease SERA5 regulates the kinetics and efficiency of malaria parasite egress from host erythrocytes. PLOS Pathog. 13:e1006453.doi: 10.1371/journal.ppat.1006453 [PubMed: 28683142]

Collins CR, Hackett F, Strath M, Penzo M, Withers-Martinez C, Baker DA, Blackman MJ. 2013; Malaria Parasite cGMP-dependent Protein Kinase Regulates Blood Stage Merozoite Secretory Organelle Discharge and Egress. PLoS Pathog. 9:e1003344.doi: 10.1371/journal.ppat.1003344 [PubMed: 23675297]

Cowman AF, Healer J, Marapana D, Marsh K. 2016; Malaria: Biology and Disease. Cell. 167:610–624. DOI: 10.1016/j.cell.2016.07.055 [PubMed: 27768886]

Crick AJ, Tiffert T, Shah SM, Kotar J, Lew VL, Cicuta P. 2013; An Automated Live Imaging Platform for Studying Merozoite Egress-Invasion in Malaria Cultures. Biophys J. 104:997–1005. DOI: 10.1016/j.bpj.2013.01.018 [PubMed: 23473482]

Das S, Hertrich N, Perrin AJ, Withers-Martinez C, Collins CR, Jones ML, Watermeyer JM, Fobes ET, Martin SR, Saibil HR, Wright GJ, Treeck M, Epp C, Blackman MJ. 2015; Processing of Plasmodium falciparum Merozoite Surface Protein MSP1 Activates a Spectrin-Binding Function Enabling Parasite Egress from RBCs. Cell Host Microbe. 18:433–444. DOI: 10.1016/j.chom.2015.09.007 [PubMed: 26468747]

de Koning-Ward TF, Gilson PR, Boddey JA, Rug M, Smith BJ, Papenfuss AT, Sanders PR, Lundie RJ, Maier AG, Cowman AF, Crabb BS. 2009; A newly discovered protein export machine in malaria parasites. Nature. 459:945–949. DOI: 10.1038/nature08104 [PubMed: 19536257]

De Niz M, Burda PC, Kaiser G, del Portillo HA, Spielmann T, Frischknecht F, Heussler VT. 2017; Progress in imaging methods: insights gained into Plasmodium biology. Nat Rev Microbiol. 15:37–54. DOI: 10.1038/nrmicro.2016.158 [PubMed: 27890922]

Dvorin JD, Martyn DC, Patel SD, Grimley JS, Collins CR, Hopp CS, Bright AT, Westenberger S, Winzeler E, Blackman MJ, Baker DA, Wandless TJ, Duraisingh MT. 2010; A Plant-Like Kinase in Plasmodium falciparum Regulates Parasite Egress from Erythrocytes. Science. 328:910–912. DOI: 10.1126/science.1188191 [PubMed: 20466936]

Feder N, Sidman RL. 1958; Methods and principles of fixation by freeze-substitution. J Biophys Biochem Cytol. 4:593–600. [PubMed: 13587555]

Flammersfeld, A; Lang, C; Flieger, A; Pradel, G. Phospholipases during membrane dynamics in malaria parasites. Int J Med Microbiol IJMM. 2017.

Frénal K, Dubremetz JF, Lebrun M, Soldati-Favre D. 2017; Gliding motility powers invasion and egress in Apicomplexa. Nat Rev Microbiol. 15:645–660. DOI: 10.1038/nrmicro.2017.86 [PubMed: 28867819]

Glushakova S, Busse BL, Garten M, Beck JR, Fairhurst RM, Goldberg DE, Zimmerberg J. 2017; Exploitation of a newly-identified entry pathway into the malaria parasite-infected erythrocyte to inhibit parasite egress. Sci Rep. 7:12250.doi: 10.1038/s41598-017-12258-x [PubMed: 28947749]

Glushakova S, Humphrey G, Leikina E, Balaban A, Miller J, Zimmerberg J. 2010; New stages in the program of malaria parasite egress imaged in normal and sickle erythrocytes. Curr Biol. 20:1117–1121. DOI: 10.1016/j.cub.2010.04.051 [PubMed: 20537541]

Glushakova S, Lizunov V, Blank PS, Melikov K, Humphrey G, Zimmerberg J. 2013; Cytoplasmic free Ca2+ is essential for multiple steps in malaria parasite egress from infected erythrocytes. Malar J. 12:41.doi: 10.1186/1475-2875-12-41 [PubMed: 23363708]

Glushakova S, Mazar J, Hohmann-Marriott MF, Hama E, Zimmerberg J. 2009; Irreversible effect of cysteine protease inhibitors on the release of malaria parasites from infected erythrocytes. Cell Microbiol. 11:95–105. DOI: 10.1111/j.1462-5822.2008.01242.x [PubMed: 19016793]

Glushakova S, Yin D, Li T, Zimmerberg J. 2005; Membrane Transformation during Malaria Parasite Release from Human Red Blood Cells. Curr Biol. 15:1645–1650. DOI: 10.1016/j.cub.2005.07.067 [PubMed: 16169486]

Guerra AJ, Carruthers VB. 2017; Structural Features of Apicomplexan Pore-Forming Proteins and Their Roles in Parasite Cell Traversal and Egress. Toxins. 9doi: 10.3390/toxins9090265

Hale VL, Watermeyer JM, Hackett F, Vizcay-Barrena G, van Ooij C, Thomas JA, Spink MC, Harkiolaki M, Duke E, Fleck RA, Blackman MJ, Saibil HR. 2017; Parasitophorous vacuole poration precedes its rupture and rapid host erythrocyte cytoskeleton collapse in Plasmodium falciparum egress. Proc Natl Acad Sci. 114:3439–3444. DOI: 10.1073/pnas.1619441114 [PubMed: 28292906]

Hall R, McBride J, Gillian M, Tait A, Zolog W, Walliker D, Scaife J. 1983; Antigens of the Erythrocytic stages of the human malaria parasite Plasmodium Falciparum detected by monoclonal antibodies. Mol Biochem Parasitol. 7:265.

Hanssen E, McMillan PJ, Tilley L. 2010; Cellular architecture of Plasmodium falciparum-infected erythrocytes. Int J Parasitol, ICOPA XII. 40:1127–1135. DOI: 10.1016/j.ijpara.2010.04.012

Heuser JE, Reese TS, Dennis MJ, Jan Y, Jan L, Evans L. 1979; Synaptic vesicle exocytosis captured by quick freezing and correlated with quantal transmitter release. J Cell Biol. 81:275–300. [PubMed: 38256]

Johnson D, Günther K, Ansorge I, Benting J, Kent A, Bannister L, Ridley R, Lingelbach K. 1994; Characterization of membrane proteins exported from Plasmodium falciparum into the host erythrocyte. Parasitology. 109:1.doi: 10.1017/S0031182000077696 [PubMed: 8058359]

Jones E, Oliphant T, Peterson P. 2001SciPy: Open Source Scientific Tools for Python.

Koch, M; Baum, J. The mechanics of malaria parasite invasion of the human erythrocyte – towards a reassessment of the host cell contribution. Cell Microbiol. 2016. n/a-n/a.

Langreth SG, Jensen JB, Reese RT, Trager W. 1978; Fine Structure of Human Malaria In Vitro. J Protozool. 25:443–452. DOI: 10.1111/j.1550-7408.1978.tb04167.x [PubMed: 105129]

Millholland MG, Chandramohanadas R, Pizzarro A, Wehr A, Shi H, Darling C, Lim CT, Greenbaum DC. 2011; The Malaria Parasite Progressively Dismantles the Host Erythrocyte Cytoskeleton for Efficient Egress. Mol Cell Proteomics. 10:M111010678.doi: 10.1074/mcp.M111.010678

Nasamu AS, Glushakova S, Russo I, Vaupel B, Oksman A, Kim AS, Fremont DH, Tolia N, Beck J, Mayers M, Jacquin N, Zimmerberg J, Goldberg D. 2017; Plasmepsins IX and X are essential and druggable mediators of malaria parasite egress and invasion. Science. 358:518–522. DOI: 10.1126/science.aan1478 [PubMed: 29074774]

Otsu N. 1979; A Threshold Selection Method from Gray-Level Histograms. IEEE Trans Syst Man Cybern. 9:62–66. DOI: 10.1109/TSMC.1979.4310076

Pino P, Caldelari R, Mukherjee B, Vahokoski J, Klages N, Maco B, Collins CR, Blackman MJ, Kursula I, Heussler V, Brochet M, Soldati-Favre D. 2017; A multistage antimalarial targets the plasmepsins IX and X essential for invasion and egress. Science. 358:522–528. DOI: 10.1126/science.aaf8675 [PubMed: 29074775]

Ruecker A, Shea M, Hackett F, Suarez C, Hirst EMA, Milutinovic K, Withers-Martinez C, Blackman MJ. 2012; Proteolytic activation of the essential parasitophorous vacuole cysteine protease SERA6 accompanies malaria parasite egress from its host erythrocyte. J Biol Chem. 287:37949–37963. DOI: 10.1074/jbc.M112.400820 [PubMed: 22984267]

Sakaguchi M, Miyazaki N, Fujioka H, Kaneko O, Murata K. 2016; Three-dimensional analysis of morphological changes in the malaria parasite infected red blood cell by serial block-face scanning electron microscopy. J Struct Biol. 193:162–171. DOI: 10.1016/j.jsb.2016.01.003 [PubMed: 26772147]

Salmon BL, Oksman A, Goldberg DE. 2001; Malaria parasite exit from the host erythrocyte: A two-step process requiring extraerythrocytic proteolysis. Proc Natl Acad Sci. 98:271–276. DOI: 10.1073/pnas.98.1.271 [PubMed: 11114161]

Schindelin J, Arganda-Carreras I, Frise E, Kaynig V, Longair M, Pietzsch T, Preibisch S, Rueden C, Saalfeld S, Schmid B, Tinevez JY, White DJ, Hartenstein V, Eliceiri K, Tomancak P, Cardona A. 2012; Fiji: an open-source platform for biological-image analysis. Nat Methods. 9:676–682. DOI: 10.1038/nmeth.2019 [PubMed: 22743772]

Shaner NC, Lambert GG, Chammas A, Ni Y, Cranfill PJ, Baird MA, Sell BR, Allen JR, Day RN, Israelsson M, Davidson MW, Wang J. 2013; A bright monomeric green fluorescent protein derived from Branchiostoma lanceolatum. Nat Methods. 10:407–409. DOI: 10.1038/nmeth.2413 [PubMed: 23524392]

Taylor HM, McRobert L, Grainger M, Sicard A, Dluzewski AR, Hopp CS, Holder AA, Baker DA. 2010; The Malaria Parasite Cyclic GMP-Dependent Protein Kinase Plays a Central Role in Blood-Stage Schizogony. Eukaryot Cell. 9:37–45. DOI: 10.1128/EC.00186-09 [PubMed: 19915077]

Thomas JA, Collins CR, Das S, Hackett F, Graindorge A, Bell D, Deu E, Blackman MJ. 2016; Development and Application of a Simple Plaque Assay for the Human Malaria Parasite Plasmodium falciparum. PloS One. 11:e0157873.doi: 10.1371/journal.pone.0157873 [PubMed: 27332706]

Thomas JA, Tan MYS, Bisson C, Borg A, Umrekar TR, Hackett F, Hale VL, Vizcay-Barrena G, Fleck RA, Snijders AP, Saibil HR, Blackman MJ. 2018; A protease cascade regulates release of the human malaria parasite Plasmodium falciparum from host red blood cells. Nat Microbiol. 1doi: 10.1038/s41564-018-0111-0

Trager W. 1956; The intracellular position of malarial parasites. Trans R Soc Trop Med Hyg. 50:419–420. [PubMed: 13360993]

van der Walt S, Schönberger JL, Nunez-Iglesias J, Boulogne F, Warner JD, Yager N, Gouillart E, Yu T, scikit-image contributors. 2014; scikit-image: image processing in Python. PeerJ. 2:e453.doi: 10.7717/peerj.453 [PubMed: 25024921]

Wickham ME, Culvenor JG, Cowman AF. 2003; Selective Inhibition of a Two-step Egress of Malaria Parasites from the Host Erythrocyte. J Biol Chem. 278:37658–37663. DOI: 10.1074/jbc.M305252200 [PubMed: 12857731]

Yeoh S, O'Donnell RA, Koussis K, Dluzewski AR, Ansell KH, Osborne SA, Hackett F, Withers-Martinez C, Mitchell GH, Bannister LH, Bryans JS, Kettleborough CA, Blackman MJ. 2007; Subcellular discharge of a serine protease mediates release of invasive malaria parasites from host erythrocytes. Cell. 131:1072–1083. DOI: 10.1016/j.cell.2007.10.049 [PubMed: 18083098]

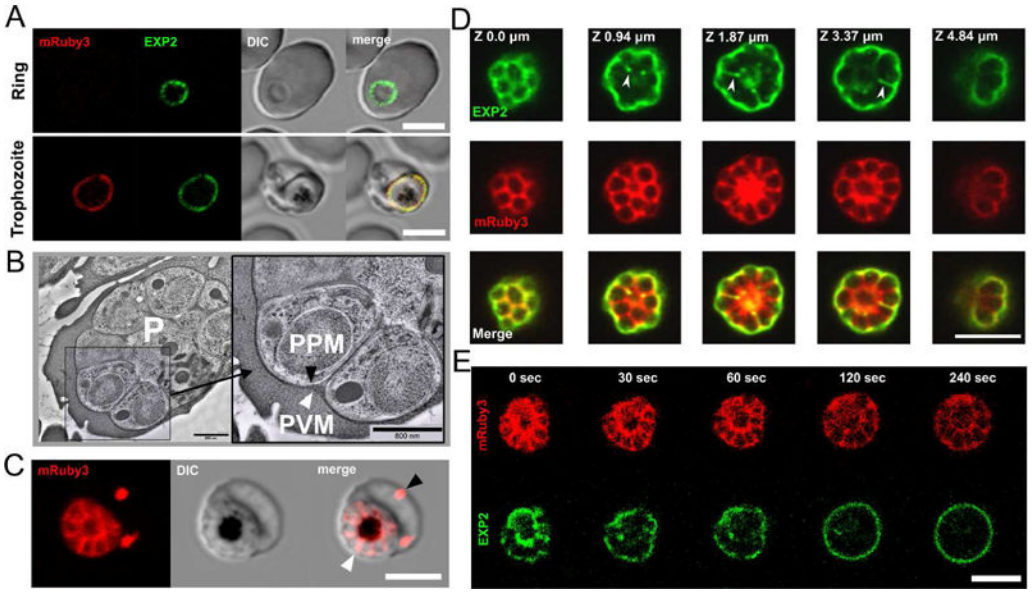

Fig.1. Visualization of parasitophorous vacuolar lumen and vacuolar membrane by light and electron microscopy

A. Visualization of the parasitophorous vacuole by detecting fluorescently tagged PVM-resident protein Exp2-mNeonGreen (green color) and soluble vacuolar fluorescent protein mRuby3 (red color) using live cell fluorescence microscopy. Note that the *de novo* produced mRuby3 peptide became visible starting from the trophozoite stage of parasite development, while Exp2 could be visualized started from the ring stage due to secretion from dense granules immediately following invasion. Both signals are co-localized in the trophozoite. B. EM images of schizont showing peripheral location of PVM during schizogony. PVM, (white arrowhead) and parasite plasma membrane (PPM, black arrowhead). P, parasite. Cryo-microscopy. Scale bar = 800 nm. C. The pattern of soluble PV-targeted mRuby3 protein distribution in the schizont stage: signal delineates *de novo* formed parasites arranged in a flower-like structure and marks both the PV compartment (white arrowhead) and the extra-parasitic membrane compartments in the erythrocyte cytoplasm (black arrowhead). D. A partial co-localization (white arrowhead) of vacuolar membrane and lumen fluorescent signals revealed in the optical sections of a schizont. Airy scan confocal microscopy. E. Photodamage and swelling of an infected erythrocyte leads to the redistribution of Exp2- mNeonGreen signal to the vacuolar periphery. Time 0: laser wounding of the erythrocyte using 800 nm two-photon illumination of the area outside the schizont location. All scale bars in the light-microscopy images are 5 µm.

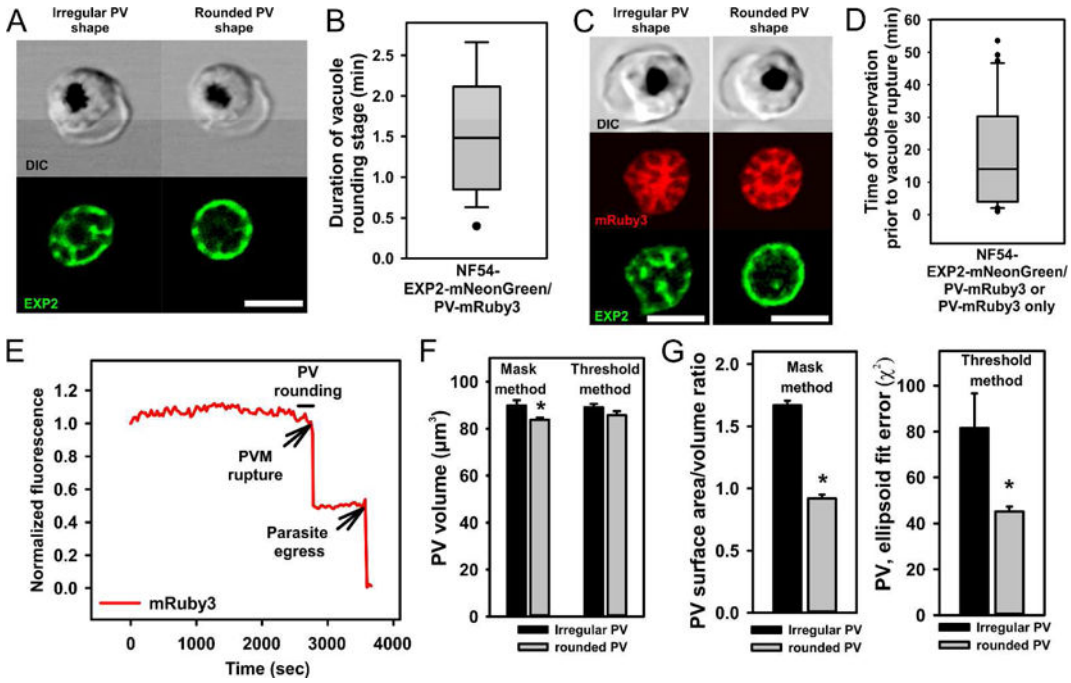

Fig.2. Transition of the irregularly shaped parasitophorous vacuole into a short-lasting rounded shape

A. A representative schizont approaching the rounded vacuole stage (left images) and during the rounded stage (right images). Note the peripheral location of Exp2-mNeonGreen signal in the rounded but not in the irregular shaped schizont/vacuole. B. The length of the rounded vacuole stage measured in 27 recordings of natural parasite egress. Double-tagged parasites were used for time-lapse recordings. Data distribution is shown as a box and whisker diagram with outliers. Mean +/−SEM=1.60+/−0.21 min. C. Irregular (left panel) and rounded-shaped (right panel) vacuole have the same high intensity of mRuby3 fluorescence (vacuolar lumen marker), indicating a preservation of PVM integrity. D. Monitoring of the vacuolar fluorescence prior to PVM rupture. Duration of live time-lapse recordings starting from the initiation of recording until the time of parasite egress (n=36). E. An example of the integrated cell fluorescence, calculated from each frame in time series and then normalized to the first time point. All cells showed a stable mRuby3 fluorescence up to the moment of PVM rupture. The second drop of fluorescence is associated with parasite egress from the infected erythrocyte. F-G. The vacuolar volume (F) and sphericity (G) calculated from fluorescence serial Z-sections of schizonts before and during the rounded stage (see Experimental procedures section). Quantitative analysis supports visual conclusion of vacuole rounding and shows a slightly diminished vacuolar volume in rounded stage schizonts (1.4% and 6.7% decrease in two independent assessment methods, n=5). All scale bars are equal 5 µm

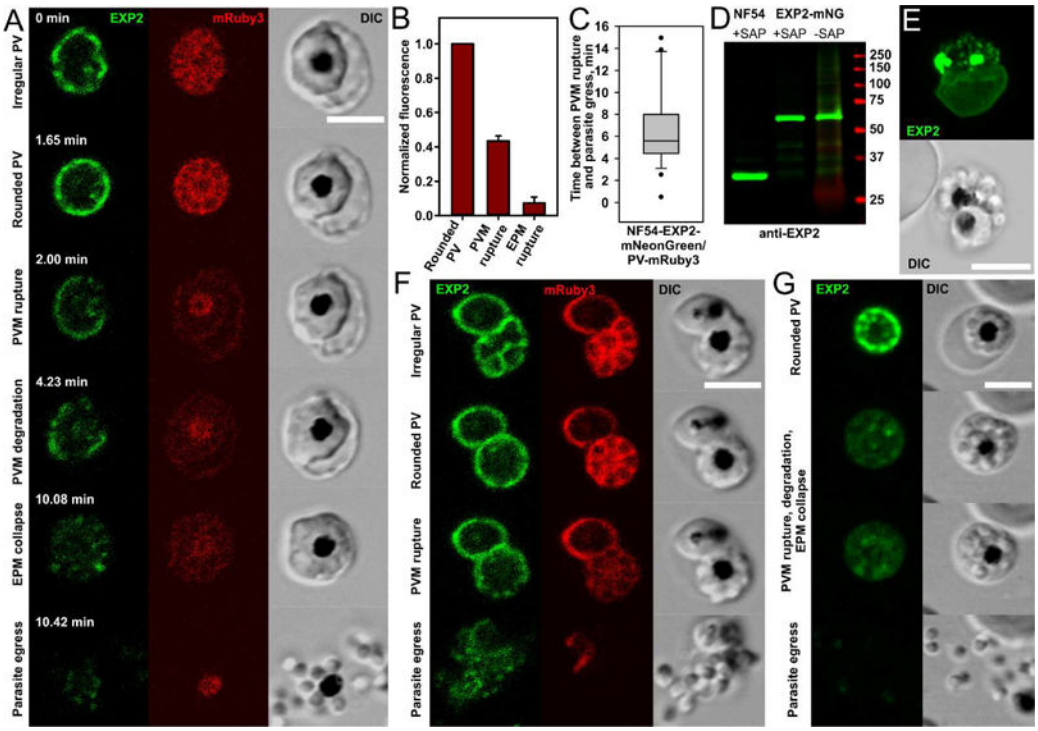

Fig.3. Rupture and degradation of vacuolar membrane and the following steps of erythrocyte membrane transformation

A. Morphologically distinct stages of parasite egress illustrated by a representative recording of parasite egress: the irregular vacuole undergoes transformation into the rounded vacuole and then suddenly ruptures and progressively degrades. This step is associated with redistribution of the vacuolar content to the entire erythrocyte (the first drop of mRuby3 fluorescence) and initiation of the gradual reshaping of the erythrocyte membrane until it collapses on the schizont body. Parasite egress (the disappearance of mRuby3 signal and dispersion of parasites) ends the replicative cycle. B. The drop of mRuby3 fluorescence (PV soluble protein) after sequential rupture of PVM and EPM. The mean fluorescence of all frames between PVM and EPM rupture (the second column) and after EPM rupture (the third column) was normalized to the mean level of fluorescence during the rounded vacuole stage (the first column); (Mean±SEM, n=12). C. Estimated time between PVM rupture and parasite egress (n=27, double labeled parasites, time-lapse recordings of parasite egress). D. Immunoblot detecting EXP2 in asynchronous NF54 parent and EXP2- mNeonGreen purified schizonts shows preservation of the fusion protein in late infected schizonts. Predicted molecular mass after signal peptide cleavage: EXP2: 30.8 kDa; EXP2-mNeonGreen: 57.8 kDa. Comparison of saponin treated (to permeabilize the EPM and PVM without solubilizing membrane proteins) and untreated samples was performed for two purposes: 1) to improve protein labeling by releasing erythrocyte hemoglobin and 2) to assess the possibility that soluble EXP2 is accumulated in membrane-bound compartments. E. Difference between the maturation times of two parasites within one erythrocyte was exploited to show that rupture and degradation of one vacuole does not affect the integrity of another vacuole. The maximum intensity projection of AiryScan Z stack images of a doubly-infected erythrocyte. Green color: Exp2-mNeonGreen. Note a diffused signal of

fluorescence from the PVM of trophozoite (lower cell) and fragmented PVM in the upper schizont. F. Rupture of one vacuole (lower right schizont) in the doubly-infected cells does not affect permeability of the second PVM (upper left trophozoite preserves mRuby3 inside the vacuole), but parasite egress from the first vacuole leads to the permeabilization or rupture of the second vacuole. G. Frames from the parasite egress time-lapse recording showing uncharacteristically early separation of parasites moving inside an erythrocyte prior to egress. All scale bars are equal 5 μm.

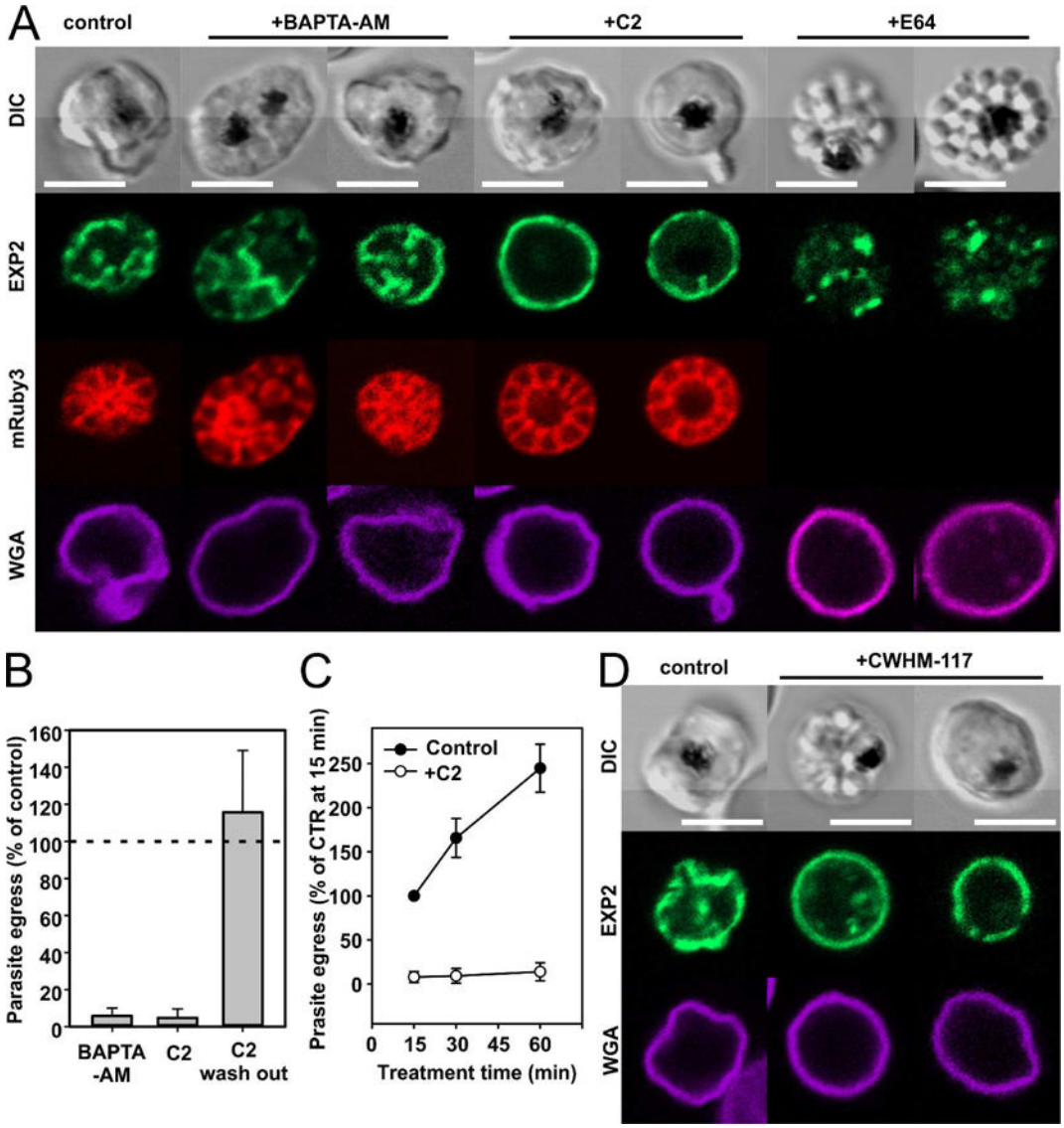

Fig.4. Effect of parasite egress inhibitors on different stages of parasite egress

A. Depletion of intracellular Ca2+ by BAPTA-AM (60 μM) blocks parasite egress prior to the rounded vacuole stage, i.e. before the earliest observable morphological transformation in an infected cell at the end of the cycle. Compound 2 (C2, 4 μM), targeting PfPKG and blocking secretion of SUB1 into the vacuole, blocks parasite egress at the rounded vacuole stage (compare with the left panel showing control schizont NF54-EXP2-mNeonGreen mRuby3). Note that the vacuole of a C2-stalled schizont is frequently enlarged but its PVM maintains its integrity (a bright mRuby3 signal inside the vacuole and absence of fluorescence in the erythrocyte compartment). E64, a cysteine protease inhibitor, blocks parasite egress by preventing rupture of the erythrocyte, but not the vacuolar membrane. Note that mRuby3 has diffused outside the cell through the perforated EPM. B. Strong inhibitory effect of BAPTA-AM and C2 on parasite egress. C2 inhibition is reversible. C. C2 has a fast and strong inhibitory effect on parasite egress. D. CWHM-117, the inhibitor of SUB1 processing, blocks NF54-PMX-KD-EXP2-mNeonGreen parasite egress at the stage

of rounded vacuole, producing stalled, distorted schizonts with apparently enlarged vacuoles. Left cell: control NF54-PMX schizont. E64, a cysteine protease inhibitor, blocks NF54-EXP2-mNeonGreen mRuby3 parasite egress by preventing rupture of the erythrocyte, but not the vacuolar membrane. At least three independent experiments were performed to evaluate the effect of drugs on parasite egress. All scale bars are equal 5 μm.

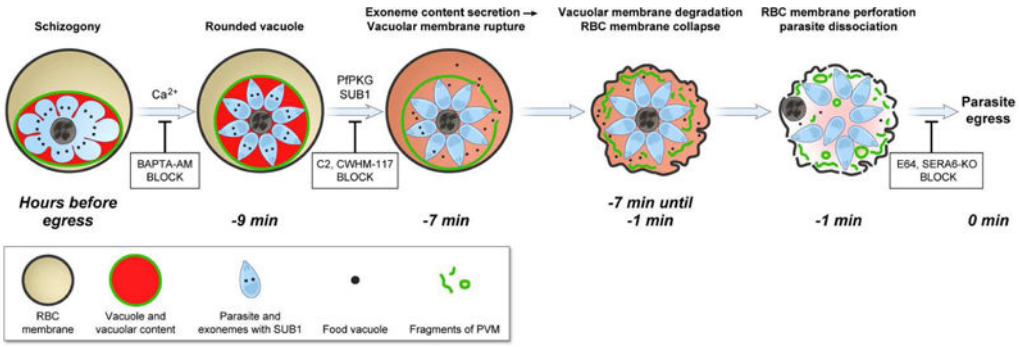

Fig.5. Known stages of parasite egress program, timing of observable events, molecular agents, and inhibitors affecting egress

A mature schizont initiates a stereotypical, Ca^{2+}-dependent egress program approximately 9 minutes prior to parasite egress. The first mechanically observable step is a rounding of the parasite vacuole lasting only a few minutes. Vacuole rounding is prevented by intracellular (but not extracellular) Ca^{2+} chelators. The rounding stage is followed by macroscopic vacuolar membrane rupture and sudden release of vacuolar contents into the erythrocyte compartment. Compounds CWHM-117 and C2 block vacuolar rupture, leaving the parasite in the vacuole rounding stage; exit from this stage apparently requires PMX-dependent SUB1 maturation and PfPKG-dependent SUB1 release from parasite exonemes. For the following ~ 7 min, the vacuolar membrane gradually degrades and the erythrocyte membrane gradually collapses on the schizont body. Two cysteine proteases, SERA 6 and host calpain-1, appear to degrade the erythrocyte cytoskeleton explaining erythrocyte shape change. The last minutes of the erythrocyte cycle is characterized by a mechanical separation of mature merozoites and perforation of erythrocyte membrane. Final parasite release completes the egress program, blocked by cysteine protease inhibitor E64 or a conditional knockout of SERA6 (SERA6-KO, Thomas et al., 2018).